JACS
JOURNAL OF THE AMERICAN CHEMICAL SOCIETY
Article
pubs.acs.org/JACS

Small-Bandgap Semiconducting Polymers with High Near-Infrared Photoresponse

Koen H. Hendriks, Weiwei Li, Martijn M. Wienk, and René A. J. Janssen*

Molecular Materials and Nanosystems, Institute for Complex Molecular Systems, Eindhoven University of Technology, P.O. Box 513, 5600 MB Eindhoven, The Netherlands

Supporting Information

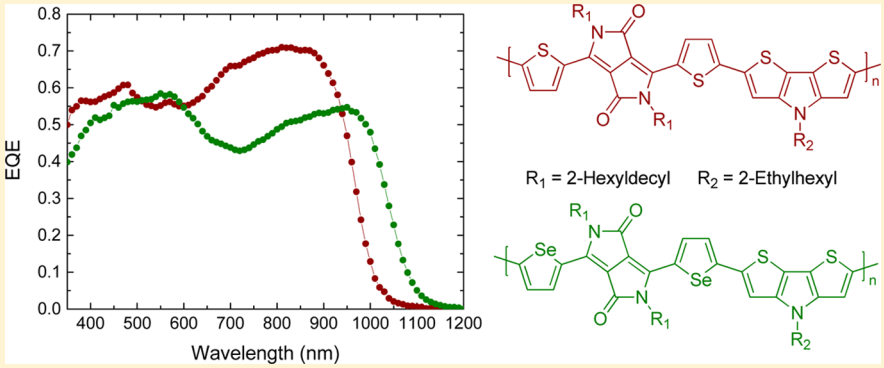

ABSTRACT: Lowering the optical bandgap of conjugated polymers while maintaining a high efficiency for photoinduced charge transfer to suitable electron acceptors such as fullerene has remained a formidable challenge in the area of organic photovoltaics. Here we present the synthesis and application of a series of ultra-small-bandgap donor−acceptor polymers composed of diketopyrrolopyrrole as acceptor and pyrrole-based groups as strong donors. The HOMO energy levels of the polymers can be progressively increased by increasing the donor strength while the LUMO level remains similar, resulting in optical bandgaps between 1.34 and 1.13 eV. Solar cells based on these polymers blended with fullerene derivatives show a high photoresponse in the near-infrared (NIR) and good photovoltaic characteristics, with power conversion efficiencies of 2.9−5.3%. The photoresponse reaches up to 50% external quantum efficiency at 1000 nm and extends to 1200 nm. With the use of a retro-reflective foil to optimize light absorption, high photocurrents up to 23.0 mA cm^{-2} are achieved under standard solar illumination conditions. These ultra-small-bandgap polymers are excellent candidates for use in multi-junction applications and NIR organic photodetectors.

INTRODUCTION

Over the past years, organic photovoltaics has emerged as an interesting field of renewable energy research. In particular, semiconducting polymer−fullerene bulk heterojunctions have received much attention. Impressive power conversion efficiencies (PCEs) in excess of 9% have been achieved for single-junction devices that utilize intermediate-bandgap absorber materials.[1−3] One of the main challenges is the intrinsically high energy loss in organic solar cells that results from the need to overcome the excitonic nature of the primary photoexcitations and produce free charges, which significantly limits the attainable PCE.[4,5] In addition, a major intrinsic energy loss originates from thermalization of excited states to the semiconductor bandgap. One way of minimizing these energy losses is by the use of a multi-junction layout, where several absorber layers with different complementary bandgaps convert the solar light into electrical energy.[6] These device layouts have already been proven successful, with PCEs up to 10.6% for a tandem device.[7] However, the optical absorption of these devices typically does not exceed ∼900 nm, while the solar spectrum extends much farther into the near-infrared (NIR). This leaves an unused part of the solar spectrum and a potential opening for further improvement of organic solar cell performance.

Semiconducting polymers with ultra-small bandgaps have been synthesized before.[8−14] However, the challenge in designing and synthesizing materials that have a good photoresponse beyond 900 nm and an appreciable PCE in polymer−fullerene solar cells lies (among others) in the precise energy level control that is required. There needs to be a sufficient energy offset between the highest occupied molecular orbital and lowest unoccupied molecular orbital (HOMO/LUMO) levels of the fullerene and the HOMO/LUMO levels of the polymer to efficiently dissociate excitons into free charges. In practice, energy offsets in the range of 0.3−0.4 eV are required in order to have optimal charge separation.[15] Especially for efficient small-bandgap polymer donors, the

Received: June 22, 2014
Published: August 7, 2014

   dx.doi.org/10.1021/ja506265h | J. Am. Chem. Soc. 2014, 136, 12130−12136

Scheme 1. Polymerization to PDPPTPyT, PDPPSPyS, PDPPTDTPT, and PDPPSDTPS

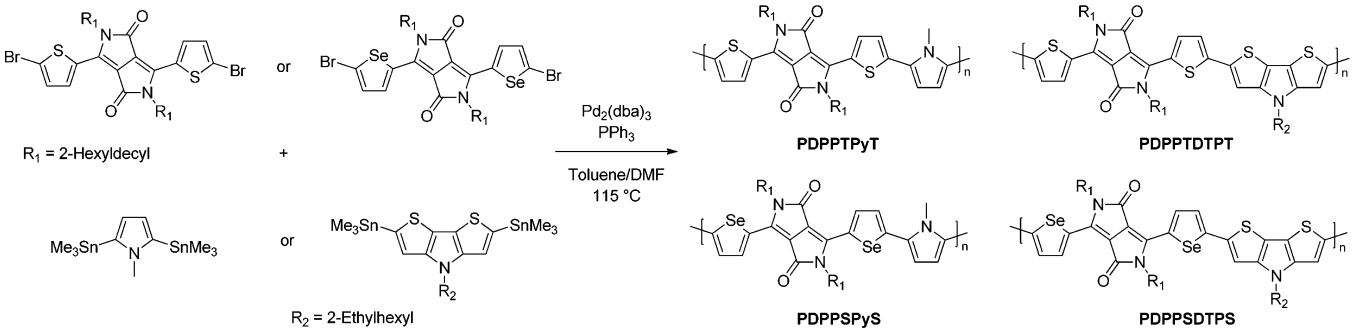

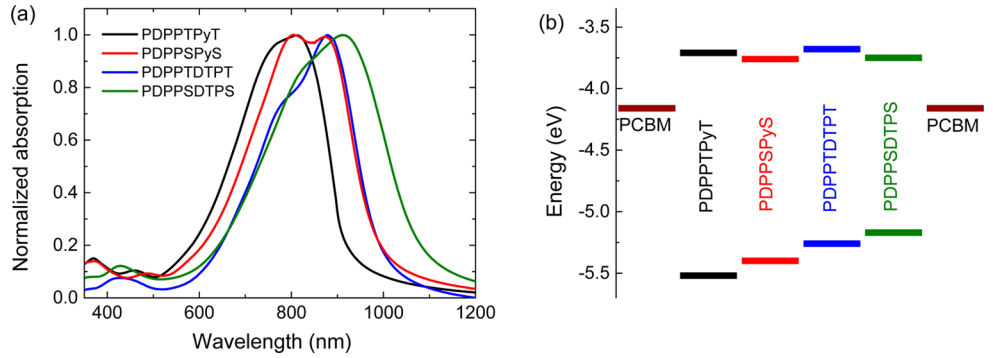

Figure 1. (a) UV/vis/NIR absorption spectra of the polymers in thin solid films. (b) Band diagram representing the HOMO and LUMO levels determined by CV, compared to the LUMO of PCBM at −4.16 eV.

minimum energy offset of the LUMO levels requires the HOMO energy level of the polymer to be very high. As the open-circuit voltage (V_{oc}) in an organic solar cell is related to the energy difference between the HOMO of the donor and the LUMO of the acceptor, this will inevitably result in small V_{oc} with small bandgaps.[16] It is therefore essential for ultra-small-bandgap polymers to have energy levels that exactly balance the bandgap with the energy loss and their overall performance in solar cells.

Here we present a series of alternating donor−acceptor (D-A) co-polymers that progressively push the bandgap down while maintaining a high photoresponse and good photovoltaic characteristics. The polymers are composed of strong electron-accepting diketopyrrolopyrrole (DPP) moieties alternating with very strong electron-donating pyrrole-based groups. Diketopyrrolopyrrole is known for its strong electron affinity and facile synthesis of high-performance semiconducting polymers with good photovoltaic performance and high hole and electron mobilities.[17−22] Pyrrole represents an electron-rich building block and has a strong foundation in organic (semi)conducting applications. However, pyrrole-based materials are often prone to oxidation and therefore can result in challenging chemistry.[23,24] Here we show a straightforward synthetic route to use *N*-methylpyrrole as a strong electron donor unit in D-A co-polymers. Furthermore, by replacing the pyrrole with an even stronger donor, dithienopyrrole, the bandgap can be further lowered by selectively increasing the HOMO energy level, while the LUMO remains unchanged.[25−28] Additionally, thiophene-to-selenophene substitution on the DPP core acts as another tool to mainly increase the HOMO energy level.[29−31] Ultimately the bandgap for these materials is tuned from 1.34 eV down to 1.13 eV while the photoresponse remains high, with up to 50% external quantum efficiency (EQE) at 1000 nm, extending to 1200 nm.

RESULTS AND DISCUSSION

The ultra-small-bandgap co-polymers were synthesized using palladium-catalyzed cross-coupling condensation polymerization of 3,6-bis(5-bromothiophen-2-yl)-2,5-bis(2-hexyldecyl)-2,5-dihydropyrrolo[3,4-*c*]pyrrole-1,4-dione or 3,6-bis(5-bromoselenophen-2-yl)-2,5-bis(2-hexyldecyl)-2,5-dihydropyrrolo[3,4-*c*]pyrrole-1,4-dione with 2,5-bis(trimethylstannyl)-*N*-methylpyrrole or 2,6-bis(trimethylstannyl)-*N*-(2-ethylhexyl)-dithieno[3,2-*b*:2,3-*d*]pyrrole according to Scheme 1. The bis-stannylpyrrole monomer was obtained from the reaction of *N*-methylpyrrole with *n*-butyllithium in the presence of tetramethylethylenediamine (TMEDA) and quenching with trimethylstannyl chloride. Although 2,5-bis(trimethylstannyl)-*N*-pyrrole is susceptible to decomposition in protic solvents, use of recrystallization from acetonitrile resulted in pure product. PDPPTPyT, PDPPSPyS, PDPPTDTPT, and PDPPSDTPS were obtained in high yields (82−97%).

Gel permeation chromatography (GPC) analysis of the materials proved to be challenging. Both PDPPTDTPT and PDPPSDTPS did not elute from the column, neither using a GPC system with *o*-dichlorobenzene at 80 °C nor a system with chloroform up to 145 °C. At this point the reason is unclear: either these particular polymers adhere to the stationary phase of the column or they deteriorate at the high temperature in chlorinated solvents. PDPPTPyT and PDPPSPyS did elute from the high-temperature GPC in chloroform, but the traces showed an elution tail and a signal originating from aggregated polymer chains at the elution limit of the column, even at 145 °C (see Supporting Information (SI), Figure S1). Therefore, no reliable values for M_n and M_w could

dx.doi.org/10.1021/ja506265h | J. Am. Chem. Soc. 2014, 136, 12130−12136

be assigned to the polymers. However, from the high yield of the polymerization reactions, the high viscosity of polymer solutions at low concentrations, and the absence of oligomer fractions during Soxhlet extractions, we deduce that the molecular weights for all batches are high and in the same order as those of other previously published polymers that were synthesized with identical procedures (M_n > 50 kg mol^{-1}).[20,32]

UV/vis/NIR spectroscopy shows that the absorption bands in the solid state progressively shift to longer wavelengths with increasing donor strength from pyrrole to dithienopyrrole and from thiophene to selenophene (Figure 1). This results in optical bandgaps (E_g) of 1.34 eV for PDPPTPyT and 1.24 eV for its selenium counterpart, 1.23 eV for PDPPTDTPT, and ultimately 1.13 eV for PDPPSDTPS (Table 1). Interestingly,

Table 1. Optical Absorption Onsets and Redox Potentials

polymer	E_{red}[a] (V)	E_{ox}[a] (V)	E(LUMO)[b] (eV)	E(HOMO)[b] (eV)	E_g (eV)
PDPPTPyT	−1.52	0.29	−3.71	−5.52	1.34
PDPPSPyS	−1.47	0.17	−3.76	−5.40	1.24
PDPPTDTPT	−1.55	0.03	−3.68	−5.26	1.23
PDPPSDTPS	−1.48	−0.06	−3.75	−5.17	1.13

[a]Versus Fc/Fc$^+$. [b]Determined using a workfunction value of −5.23 eV for Fc/Fc$^+$.

the two polymers with selenophene both show a large red-shift on going from solution to the film, while for the thiophene analogues this is not observed (SI, Figure S2).

Cyclic voltammetry (CV) measurements on thin films (SI, Figure S3) were performed to estimate the frontier orbital energy levels of the polymers, from the onset of the oxidation (E_{ox}) and reduction (E_{red}) waves (Table 1). Although the bandgap derived from CV is systematically higher than the one obtained from optical measurements, the same trend is observed. The main difference between the polymers is a gradual increase of the HOMO energy level. The LUMO energy level is very similar for all materials, but the selenophene materials have a slightly lower LUMO compared to the thiophene analogues. Likewise, going from pyrrole to dithienopyrrole as a donor, the main difference is an increase of the HOMO energy level.

Hole mobilities were measured in a field-effect transistor configuration with a heavily doped Si bottom gate electrode, a SiO_2 dielectric, and Au bottom source and drain contacts. The hole mobilities of the four polymers were found to be very similar, ranging from 2.5 × 10^{-2} to 8.0 × 10^{-2} cm^2 V^{-1} s^{-1} (SI, Figure S4). These values are consistent with hole mobilites of related DPP-based polymers measured under identical conditions.[33]

The photovoltaic performance of the materials was evaluated in solar cells with the active layer consisting of a blend of polymer and phenyl-C_{61}-butyric acid methyl ester ([60]-PCBM), sandwiched between a transparent indium tin oxide (ITO) front electrode covered with poly(ethylenedioxythiophene):poly(styrenesulfonate) (PEDOT:PSS) and a reflective LiF/Al back electrode. For every polymer, the blend layer was carefully optimized in terms of polymer-to-fullerene ratio, amount and type of co-solvent used for spin-coating, and active layer thickness in order to maximize the PCE. The characteristics of the optimal devices are summarized in Figure 2 and Table 2.

The V_{oc} of the cells clearly reflects the trend of the HOMO energy levels determined by the CV measurements, going down from 0.55 V for PDPPTPyT to 0.48 V for PDPPSPyS and from 0.43 for PDPPTDTPT to 0.34 V for PDPPSDTPS. Most cells show good fill factor (FF) values, especially when considering the low V_{oc} values; only PDPPSPyS shows slightly lower FF, which is probably caused by a poorer morphology. Transmission electron microscopy (TEM) analysis of the optimized photovoltaic blends shows that for PDPPSPyS no clear fibrillar structures are observed, while these are present in the other blends (SI, Figure S6). These fibrils are favorable for charge transport and can explain the difference in FF that is observed for the different blends.[32]

EQE spectra measured for the solar cells show high photoresponse of the polymers, especially in the NIR region, where the maximum EQE exceeds 0.45 for all blends (Figure 2b). Integrating the EQE of PDPPTPyT and PDPPSPyS with the AM1.5G reference solar spectrum yields high short-circuit currents (J_{sc}) of 14.0 and 12.9 mA cm^{-2}, respectively. The difference in heights of the photoresponses between these materials seems to be primarily due to a lower absorption coefficient of PDPPSPyS compared to its thiophene analogue (SI, Figure S7). The slightly larger offset of the LUMO levels for PDPPTPyT can also help increase the quantum efficiency in the polymer absorption region.[33] Notable is the performance of PDPPSDTPS, which retains a very high overall EQE with an optical gap of only 1.13 eV. This results in an extended response up to 1200 nm and high J_{sc} = 15.4 mA cm^{-2}. PDPPTDTPT has an even larger EQE$_{max}$ = 0.58 and J_{sc} = 15.5

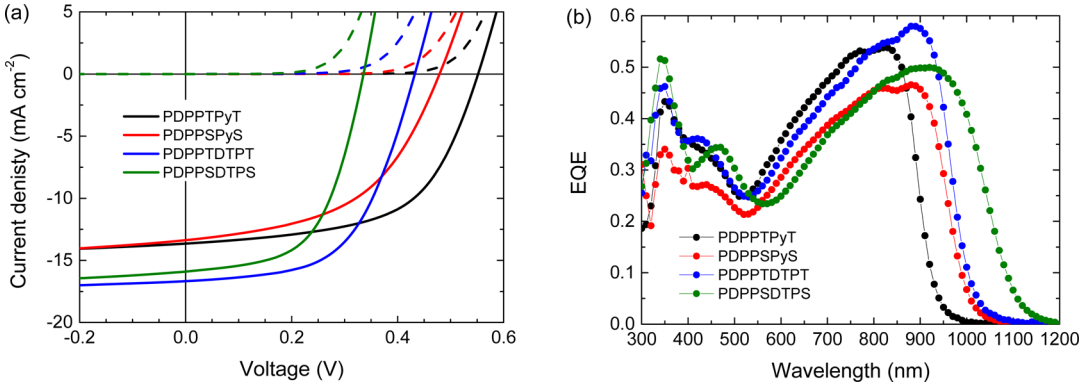

Figure 2. (a) J−V curves of regular configuration polymer/[60]PCBM solar cells in the dark (dashed lines) and under illumination (solid lines). Extended-scale J−V curves are shown in the SI as Figure S5. (b) The corresponding EQE spectra.

dx.doi.org/10.1021/ja506265h | J. Am. Chem. Soc. 2014, 136, 12130−12136

Table 2. Solar Cell Characteristics of Regular Configuration Polymer/[60]PCBM Devices

polymer	d (nm)	V_{oc} (V)	J_{sc}[a] (mA cm^{-2})	FF	EQE$_{max}$	$E_g - eV_{oc}$ (eV)	IQE$_{av}$	PCE (%)
PDPPTPyT	114	0.55	14.0	0.58	0.54	0.79	0.74	4.5
PDPPSPyS	115	0.48	12.9	0.50	0.47	0.76	0.66	3.1
PDPPTDTPT	117	0.43	15.5	0.56	0.58	0.80	0.73	3.8
PDPPSDTPS	124	0.34	15.4	0.57	0.50	0.79	0.74	2.9

[a]Determined by integrating the EQE spectrum with the AM1.5 G spectrum.

mA cm^{-2}. This difference is again attributed to a larger absorption coefficient of the thiophene analogue and a slightly higher energy offset to the LUMO of [60]PCBM. The photoresponse of PDPPTDTPT is noticeably higher than previously reported for polymers with an identical backbone structure.[25,27] This is most likely a result of the higher molecular weight of the polymer in combination with a different substitution pattern of the alkyl side chains. This polymer is processed at a concentration of only 3 mg mL^{-1}, and even then, after heating, gelation of the solution sets in after a few minutes. From our experience, this is due to the presence of high-molecular-weight polymer chains, which are in general beneficial for solar cell performance.[20,34−36] The other materials did not show this extreme gelation behavior but still showed impressively high EQE spectra. Overall these high responses lead to good PCEs between 2.9 and 4.5%.

In terms of the minimum photon energy loss of the cells, as defined by $E_g - eV_{oc}$ (with e the elementary charge), all polymers have similar losses of around 0.80 eV. As a lower limit of 0.6 eV has been established as a threshold for efficient device operation, these materials still lose additional energy in converting photons to electrons.[16] However, this larger energy loss is reflected in the high photoresponse which is crucial for multi-junction applications where series-connected sub-cells need to be current-matched.[6,33]

Using the wavelength-dependent refractive index $n(\lambda)$ and extinction coefficient $k(\lambda)$ determined for the polymer/fullerene blends, the absorption of light by the active layer was modeled and the average internal quantum efficiency (IQE) calculated. IQE values well over 0.7 were found for three materials. This is high and follows the trend of EQE$_{max}$ for each blend. Only PDPPSPyS had an average IQE < 0.7, which is attributed to the sub-optimal morphology. Modeling results also showed that the relative large difference between the internal and external quantum efficiencies is mainly due to sub-optimal light absorption in the active layer, especially in the NIR region. This is due to parasitic absorption in the polaron band of PEDOT:PSS and the use of aluminum as a back reflector (Figure 3), which absorbs some of the NIR light after the first pass, limiting the amount of photons that are absorbed by the active layer.

Inverted polarity device configurations use low light-absorbing metal oxides, e.g., ZnO as electron transport layer (ETL) and MoO_3 as hole transport layer (HTL) with silver as a back reflector, which is superior compared to aluminum. The absorption profiles are shown in Figure 3: the optical electric field is enhanced in the inverted configuration, which results in more photons being absorbed. Hence, higher photocurrents can be expected.

Inverted devices were fabricated using the same active layer formulations but changing the ETL and HTL. Unfortunately, blends of PDPPTPyT and PDPPSPyS with [60]PCBM displayed an S-shaped $J-V$ curve with all electrode combinations in the inverted configuration (SI, Figure S8). The S-shape

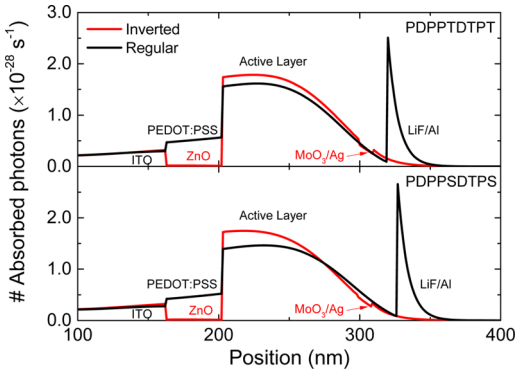

Figure 3. Modeled AM1.5G photon absorption profiles within the device stack for PDPPTDTPT/[60]PCBM and PDPPSDTPS/[60]PCBM in regular and inverted configurations.

was present for interlayers based on ZnO sol−gel, ZnO nanoparticles, poly[(9,9-bis(3′-(*N*,*N*-dimethylamino)propyl)-2,7-fluorene)-*alt*-2,7-(9,9-dioctylfluorene)] (PFN), and ethoxylated polyethylenimine (PEIE) on ITO. We tentatively assign this to vertical phase segregation, leading to pure fullerene domains on the top surface or pure polymer regions at the bottom contact, giving rise to an injection barrier when processed in an inverted configuration. Therefore, we focus on PDPPTDTPT and PDPPSDTPS, which do not display S-shapes (Figure 4a). The EQE spectra of these devices show the distinct difference between the two device configurations (Figure 4b). Because more light is absorbed in the photoactive layer of the inverted structures, EQE$_{max}$ increased by 12% for PDPPTDTPT and 18% for PDPPSDTPS. This leads to an effective increase of almost 2 mA cm^{-2} in short-circuit current, resulting in J_{sc} = 17.3 and 16.7 mA cm^{-2}, respectively (Table 3). The FF and V_{oc} remain similar to those of the regular devices, resulting in an increase of the PCE to 4.4% and 3.1%. The extended photoresponse up to 1200 nm, with a 50% EQE at 1000 nm, is the highest NIR photoresponse reported to date for organic solar cells. The IQE is higher than in the regular configuration, due to the lower optimal thickness of the active layer. Thinner active layers show, in general, less bimolecular recombination and give rise to a higher IQE.

To fully maximize the short-circuit current of devices with these polymers, inverted configuration solar cells with active layers of polymer and phenyl-C$_{71}$-butyric acid methyl ester ([70]PCBM) as the acceptor were made. The higher optical absorption coefficient of [70]PCBM aids in the generation of charges in the visible region. In addition, a retro-reflective foil was used. This foil effectively couples light into the device at an angle, increasing the optical path length while simultaneously reducing out-coupling of light from the device.[37] The enhanced light in-coupling is clearly reflected in the EQE, which displays an increased response over the whole width of the absorption. $J-V$ characteristics of the cells show that the use of [70]PCBM provides an increase in photocurrent of 3.2 mA cm^{-2} for

dx.doi.org/10.1021/ja506265h | J. Am. Chem. Soc. 2014, 136, 12130−12136

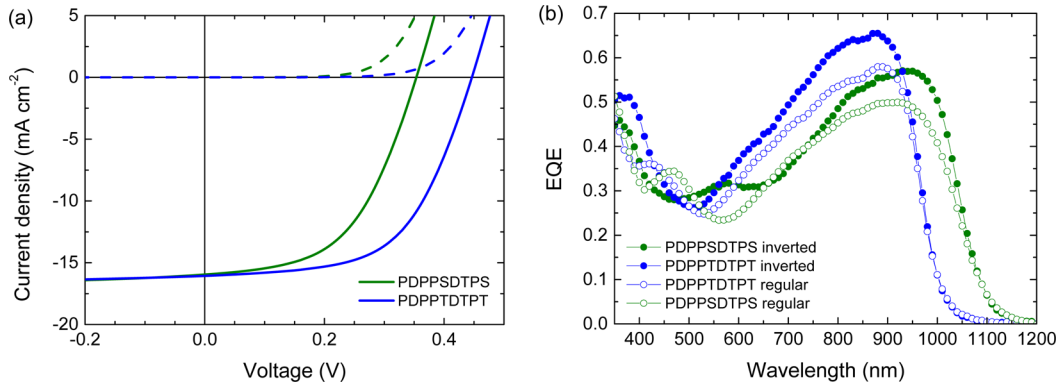

Figure 4. (a) $J-V$ curves of inverted configuration polymer/[60]PCBM solar cells in the dark (dashed lines) and under illumination (solid lines). Extended scale $J-V$ curves are shown in the SI as Figure S9. (b) The corresponding EQE spectra.

Table 3. Solar Cell Characteristics of Inverted Configuration Polymer/[60]PCBM Devices

polymer	d (nm)	V_{oc} (V)	J_{sc}[a] (mA cm^{-2})	FF	EQE$_{max}$	IQE$_{av}$	PCE (%)
PDPPTDTPT	97	0.45	17.3	0.57	0.65	0.77	4.4
PDPPSDTPS	96	0.35	16.7	0.52	0.57	0.74	3.1

[a]Determined by integrating the EQE spectrum with the AM1.5G spectrum.

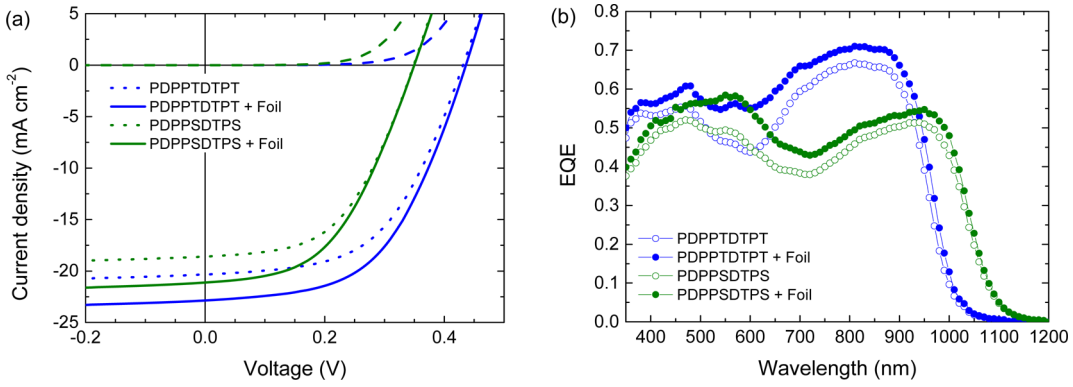

Figure 5. (a) $J-V$ curves of inverted configuration polymer/[70]PCBM solar cells in the dark (dashed lines) and under illumination with (solid lines) and without retro-reflective foil (dotted lines). Extended-scale $J-V$ curves are shown in the SI as Figure S10. (b) Corresponding EQE spectra.

PDPPTDTPT and 1.9 mA cm^{-2} for PDPPSDTPS compared to using [60]PCBM (Figure 5, Table 4). We attribute the relatively smaller increase in current for PDPPSDTPS to a slightly different morphology when changing fullerenes. Applying the retro-reflective foil on top of the cells further increases the photocurrent by another 10% to 23.0 mA cm^{-2} for PDPPTDTPD and 20.8 mA cm^{-2} for PDPPSDTPS (Figure 5, Table 4). We have previously analyzed and modeled the effects of the retro-reflective foil for polymer/[60]PCBM solar cells in detail and showed that largest improvements are obtained in spectral ranges with low absorption, but that even in the absorption maximum the light capture can be improved.[37] The EQE data shown in Figure 5b are consistent with this conclusion.

Table 4. Solar Cell Characteristics of Inverted Configuration Polymer/[70]PCBM Devices with and without Retro-reflective Foil

polymer	d (nm)	V_{oc} (V)	J_{sc}[a] (mA cm^{-2})	FF	EQE$_{max}$	PCE (%)
PDPPTDTPT	110	0.43	20.5	0.54	0.67	4.8
+ foil		0.44	23.0	0.53	0.71	5.3
PDPPSDTPS	98	0.35	18.6	0.52	0.51	3.3
+ foil		0.35	20.8	0.49	0.55	3.5

[a]Determined by integrating the EQE spectrum with the AM1.5G spectrum.

The values of J_{sc} = 23.0 and 20.8 mA cm^{-2} are among the highest reported photocurrents for bulk heterojunction organic solar cells. Despite the high photocurrents, the FF is only reduced marginally with the use of the retro-reflective foil, and the V_{oc} remains identical, resulting in maximum PCEs of 5.3% for PDPPTDTPT/[70]PCBM and 3.5% for PDPPSDTPS/[70]PCBM.

CONCLUSIONS

We have shown that semiconducting copolymers based on electron-rich segments consisting of pyrrole combined with thiophene or selenophene, alternating with electron-deficient diketopyrrolepyrrole units, represent small-bandgap materials tailored to exhibit a high photoresponse in the NIR region in solar cells when blended with fullerenes. Several factors contribute to the high NIR response for these small-bandgap DPP polymer solar cells.

dx.doi.org/10.1021/ja506265h | J. Am. Chem. Soc. 2014, 136, 12130−12136

First and foremost is the positioning of the energy levels, in particular HOMO, LUMO, and optical bandgap. For an internal quantum efficiency, a sufficiently large offset between the LUMO levels of the donor and acceptor should exist. With LUMO levels at about −3.7 eV (Table 1), these DPP polymers have an energy offset of about 0.5 eV from the LUMO level of PCBM (at −4.2 eV). This is somewhat larger than the minimum offset of 0.3−0.4 eV.[15] This is also reflected in the $E_g - eV_{oc}$ energy difference of about 0.8 eV for these cells (Table 2). Again, this is more than the minimum required 0.6 eV.[16] Although these larger offsets cause a concomitant loss in open-circuit voltage, they contribute—in practice—to a higher internal quantum efficiency.[33]

Second, the use of efficient polymerization reactions provides polymers with high performance in organic photovoltaic devices. The synthetic route and catalyst used here are known to provide DPP polymers with very few homocoupling defects and high molecular weights.[38] Both are known to contribute to a high quantum efficiency[38] and charge mobility. To fully exploit these intrinsic advantages, careful optimization of the processing conditions (concentration, weight ratio, solvent additive) to control the blend morphology is imperative.

Third, optical effects are important. For a high NIR photoresponse, it is important to exclude parasitic absorption of NIR light by electrode and interface materials such as Al and PEDOT:PSS. Figure 3 clearly shows the enhanced optical absorption by the photoactive layer of an inverted structure with ZnO and MoO_3/Ag compared to PEDOT:PSS and LiF/Al. Also the use of the retro-reflective foil is effective in enhancing light absorption. Optimizing the optical field within the devices has proven to be beneficial to further enhance the external quantum efficiency in the NIR region. In an inverted device configuration with a silver back electrode, blends of PDPPTDTPT and PDPPSDTPS with [70]PCBM provide high short-circuit currents (up to 23 mA cm^{-2}) when using a retro-reflective optical foil to improve absorption of light.

The high photoresponse in the NIR that extends up to 1200 nm opens up possibilities for applying these polymers in multi-junction solar cells and in NIR organic photodetectors.

■ ASSOCIATED CONTENT

Supporting Information

Experimental details, synthetic procedures, gel permeation chromatograms, cyclic voltammograms, transistor characteristics, optical constants, TEM images of the blends, and $J-V$ curves over extended bias and current ranges. This material is available free of charge via the Internet at http://pubs.acs.org.

■ AUTHOR INFORMATION

Corresponding Author

r.a.j.janssen@tue.nl

Notes

The authors declare no competing financial interest.

■ ACKNOWLEDGMENTS

We thank Dr. Marie-France Falzon for her primary work on pyrrole-containing small-bandgap polymers and Mr. Christian Roelofs for measuring hole mobilities. The work was performed in the framework of the Largecells and X10D projects that received funding from the European Commission's Seventh Framework Programme (Grant Agreement No. 261936 and No. 287818). The work was further supported by the "Europees Fonds voor Regionale Ontwikkeling" (EFRO) in the Interreg IV A project "Organext". The research forms part of the Solliance OPV program and has received funding from the Ministry of Education, Culture and Science (Gravity program 024.001.035).

■ REFERENCES

(1) He, Z. C.; Zhong, C. M.; Su, S. J.; Xu, M.; Wu, H. B.; Cao, Y. *Nat. Photonics* **2012**, *6*, 591−595.
(2) Ye, L.; Zhang, S.; Zhao, W.; Yao, H.; Hou, J. *Chem. Mater.* **2014**, *26*, 3603−3605.
(3) Nguyen, T. L.; Choi, H.; Ko, S.-J.; Uddin, M. A.; Walker, B.; Yum, S.; Jeong, J.-E.; Yun, M. H.; Shin, T. J.; Hwang, S.; Kim, J. Y.; Woo, H. Y. *Energy Environ. Sci.* **2014**, DOI: 10.1039/C4EE01529K.
(4) Dou, L.; You, J.; Hong, Z.; Xu, Z.; Li, G.; Street, R. A.; Yang, Y. *Adv. Mater.* **2013**, *25*, 6642−6671.
(5) Janssen, R. A. J.; Nelson, J. *Adv. Mater.* **2013**, *25*, 1847−1858.
(6) Ameri, T.; Lia, N.; Brabec, C. J. *Energy Environ. Sci.* **2013**, *6*, 2390−2413.
(7) You, J.; Dou, L.; Yoshimura, K.; Kato, T.; Ohya, K.; Moriarty, T.; Emery, K.; Chen, C.-C.; Gao, J.; Li, G.; Yang, Y. *Nat. Commun.* **2013**, *4*, 1446.
(8) Steckler, T. T.; Henriksson, P.; Mollinger, S.; Lundin, A.; Salleo, A.; Andersson, M. R. *J. Am. Chem. Soc.* **2014**, *136*, 1190−1193.
(9) Karakawa, M.; Aso, Y. *Macromol. Chem. Phys.* **2013**, *214*, 2388−2397.
(10) Yuen, J. D.; Wudl, F. *Energy Environ. Sci.* **2013**, *6*, 392−406.
(11) Fan, J.; Yuen, J. D.; Wang, M.; Seifter, J.; Seo, J.-H.; Mohebbi, A. R.; Zakhidov, D.; Heeger, A.; Wudl, F. *Adv. Mater.* **2012**, *24*, 2186−2190.
(12) Tam, T. L. D.; Salim, T.; Li, H.; Zhou, F.; Mhaisalkar, S. G.; Su, H.; Lam, Y. M.; Grimsdale, A. C. *J. Mater. Chem.* **2012**, *22*, 18528−18534.
(13) Wang, E.; Hou, L.; Wang, Z.; Hellström, S.; Mammo, W.; Zhang, F.; Inganäs, O.; Andersson, M. R. *Org. Lett.* **2010**, *12*, 4470−4473.
(14) Zoombelt, A. P.; Fonrodona, M.; Wienk, M. M.; Sieval, A. B.; Hummelen, J. C.; Janssen, R. A. J. *Org. Lett.* **2009**, *11*, 903−906.
(15) Servaites, J. D.; Ratner, M. A.; Marks, T. J. *Energy Environ. Sci.* **2011**, *4*, 4410−4422.
(16) Veldman, D.; Meskers, S. C. J.; Janssen, R. A. J. *Adv. Funct. Mater.* **2009**, *19*, 1939−1948.
(17) Li, Y.; Sonar, P.; Murphy, L.; Honga, W. *Energy Environ. Sci.* **2013**, *6*, 1684−1710.
(18) Chang, W.-H.; Gao, J.; Dou, L.; Chen, C.-C.; Liu, Y.; Yang, Y. *Adv. Energy Mater.* **2014**, *4*, 1300864.
(19) Sun, B.; Hong, W.; Yan, Z.; Aziz, H.; Li, Y. *Adv. Mater.* **2014**, *26*, 2636−2642.
(20) Hendriks, K. H.; Heintges, G. H. L.; Gevaerts, V. S.; Wienk, M. M.; Janssen, R. A. J. *Angew. Chem., Int. Ed.* **2013**, *52*, 8341−8344.
(21) Yiu, A. T.; Beaujuge, P. M.; Lee, O. P.; Woo, C. H.; Toney, M. F.; Fréchet, J. M. J. *J. Am. Chem. Soc.* **2012**, *134*, 2180−2185.
(22) Ye, L.; Zhang, S.; Ma, W.; Fan, B.; Guo, X.; Huang, Y.; Ade, H.; Hou, J. *Adv. Mater.* **2012**, *24*, 6335−6341.
(23) Kumar, D.; Sharma, R. C. *Eur. Polym. J.* **1998**, *34*, 1053−1060.
(24) Wang, L.-X.; Li, X.-G.; Yang, Y.-L. *React. Funct. Polym.* **2001**, *47*, 125−139.
(25) Zhou, E.; Wei, Q.; Yamakawa, S.; Zhang, Y.; Tajima, K.; Yang, C.; Hashimoto, K. *Macromolecules* **2010**, *43*, 821−826.
(26) Nelson, T. L.; Young, T. M.; Liu, J.; Mishra, S. P.; Belot, J. A.; Balliet, C. L.; Javier, A. E.; Kowalewski, T.; McCullough, R. D. *Adv. Mater.* **2010**, *22*, 4617−4621.
(27) Zhou, E.; Yamakawa, S.; Tajima, K.; Yang, C.; Hashimoto, K. *Chem. Mater.* **2009**, *21*, 4055−4061.
(28) Burkhart, B.; Khlyabich, P. P.; Thompson, B. C. *J. Photon. Energy* **2012**, *2*, 021002.

(29) Shahid, M.; McCarthy-Ward, T.; Labram, J.; Rossbauer, S.; Domingo, E. B.; Watkins, S. E.; Stingelin, N.; Anthopoulos, T. D.; Heeney, M. *Chem. Sci.* **2012**, *3*, 181−185.
(30) Dou, L.; Chang, W.-H.; Gao, J.; Chen, C.-C.; You, J.; Yang, Y. *Adv. Mater.* **2013**, *25*, 825−831.
(31) Ballantyne, A. M.; Chen, L. C.; Nelson, J.; Bradley, D. D. C.; Astuti, Y.; Maurano, A.; Shuttle, C. G.; Durrant, J. R.; Heeney, M.; Duffy, W.; Mcculloch, I. *Adv. Mater.* **2007**, *19*, 4544−4547.
(32) Li, W. W.; Hendriks, K. H.; Furlan, A.; Roelofs, W. S. C.; Wienk, M. M.; Janssen, R. A. J. *J. Am. Chem. Soc.* **2013**, *135*, 18942−18948.
(33) Li, W. W.; Roelofs, W. S. C.; Wienk, M. M.; Janssen, R. A. J. *J. Am. Chem. Soc.* **2012**, *134*, 13787−13795.
(34) Bijleveld, J. C.; Zoombelt, A. P.; Mathijssen, S. G. J.; Wienk, M. M.; Turbiez, M.; de Leeuw, D. M.; Janssen, R. A. J. *J. Am. Chem. Soc.* **2009**, *131*, 16616−16617.
(35) Coffin, R. C.; Peet, J.; Rogers, J.; Bazan, G. C. *Nat. Chem.* **2009**, *1*, 657−661.
(36) Wakim, S.; Beaupré, S.; Blouin, N.; Aich, B.-R.; Rodman, S.; Gaudiana, R.; Tao, Y.; Leclerc, M. *J. Mater. Chem.* **2009**, *19*, 5351−5358.
(37) Esiner, S.; Bus, T.; Wienk, M. M.; Hermans, K.; Janssen, R. A. J. *Adv. Energy Mater.* **2013**, *3*, 1013−1017.
(38) Hendriks, K. H.; Li, W. W.; Heintges, G. H. L.; van Pruissen, G. W. P.; Wienk, M. M.; Janssen, R. A. J. *J. Am. Chem. Soc.* **2014**, *136*, 11128−11133.